

# Mechanical cryocooler noise observed in the ground testing of the *Resolve* X-ray microcalorimeter onboard XRISM

R. Imamura, H. Awaki, M. Tsujimoto, S. Yamada, F. S. Porter, C. A. Kilbourne, R. L. Kelley, Y. Takei, on behalf of the XRISM *Resolve* team

Received: date / Accepted: date

**Abstract** Low-temperature detectors often use mechanical coolers as part of the cooling chain in order to reach sub-Kelvin operating temperatures. The microphonics noise caused by the mechanical coolers is a general and inherent issue for these detectors. We have observed this effect in the ground test data obtained with the *Resolve* instrument to be flown on the XRISM satellite. *Resolve* is a cryogenic X-ray microcalorimeter spectrometer with a required energy resolution of 7 eV at 6 keV. Five mechanical coolers are used to cool from ambient temperature to  $\sim 4$  K: four two-stage Stirling coolers (STC) driven nominally at 15 Hz and a Joule-Thomson cooler (JTC) driven nominally at 52 Hz. In 2019, we operated the flight-model instrument for two weeks, in which we also obtained accelerometer data inside the cryostat at a low-temperature stage (He tank). X-ray detector and accelerometer data were obtained continuously while changing the JTC drive frequency, which produced a unique data set for investigating how the vibration from the cryocoolers propagates to the detector. In the detector noise spectra, we observed harmonics of both STCs and JTC. More interestingly, we also observed the low ( $< 20$  Hz) frequency beat between the 4'th JTC and 14'th STC harmonics and the 7'th JTC and the 23–24'th STC harmonics. We present here a description and interpretation of these measurements.

**Keywords** X-ray microcalorimeter, microphonics, XRISM

## 1 Introduction

Low-temperature detectors are cooled by a multi-stage cooling system often containing mechanical coolers. The propagation of the mechanical vibration to the detector is potentially a serious source of noise. An example is the X-ray microcalorimeter instrument (Soft X-ray Spectrometer<sup>1,2</sup>; SXS) on board the Astro-H satellite<sup>3</sup>. The noise due to vibration from the mechanical coolers caused unacceptable degradation of the detector performance during ground testing. This was mitigated by installing a vibration isolation system (VIS) between the mechanical coolers and the cryostat at a very late stage of the mission<sup>4</sup>. After the launch in February 2016, the SXS achieved a stable and unprecedented performance in orbit<sup>5,6</sup> but was suddenly discontinued due to the malfunction of the spacecraft attitude control system.

Department of Physics, Ehime University, Matsuyama, Ehime, 790-8577, Japan  
E-mail: imamura@astro.phys.sci.ehime-u.ac.jp



The detector assembly<sup>14</sup> and the ADR stages are installed in the cryostat<sup>8,15,16</sup>. The He tank stores 30 liters of superfluid He surrounded by several layers of shields: Joule-Thomson shield (JTS), inner, middle, and outer vapor cooled shields (IVCS, MVCS, and OVCS, respectively), and the Dewar main shell (DMS). The shields are mechanically suspended by straps<sup>16</sup>. The He is filled and vented through plumbing with access ports and valves. When the liquid He is depleted, the system continues to operate in a cryogen-free mode utilizing a third ADR<sup>17</sup>.

Two sets of two-stage Stirling coolers (STC) and one Joule-Thomson cooler (JTC) are used<sup>18</sup>; one STC set (SC-A and B) is for cooling the OVCS and IVCS and the JTC for cooling the JTS. The other STC set (PC-A and B) is used for pre-cooling the JTC. The VIS is installed between the cryostat and each one of the compressors of the four STCs attached to the DMS. The VIS was not installed for JTC as it is known to produce line-dominated vibration noise spectra, which can be adjusted later by the change of the drive frequency. The four STCs are nominally driven at  $f_{\text{STC}} = 15.0$  Hz and the JTC at  $f_{\text{JTC}} = 52.0$  Hz by the cooler driver electronics. To avoid possible noise interference in the instrument, the drivers can change the frequency from 13.93–16.26 Hz with 256 steps at a resolution  $\Delta f_{\text{STC}} = 0.01$  Hz for the STCs and from 50.4–53.8 Hz with 32 steps at  $\Delta f_{\text{JTC}} = 0.1$  Hz for the JTC.

### 3 Measurements

A cryogenic test was conducted in 2019 December using the flight-model cryocoolers and the partially assembled cryostat including the flight model detector assembly and ADRs in order to verify that the hardware was ready for the final integration. The test was conducted in the Niihama Works of Sumitomo Heavy Industries for two weeks. A three-axis set of cryogenic accelerometers was temporarily installed on the He tank for this test. We measured  $x$ ,  $y$ , and  $z$  axis acceleration at the top of the He tank using a set of model 876 accelerometers from Columbia Research Industries, Inc. The accelerometers were sampled at 10 kHz with 32 s records, continuously, to cover the frequency range of 31.25 mHz–5 kHz with a dynamic range of  $\sim 100$  dB and a noise floor of  $2\text{--}3 \times 10^{-5} \text{ G}/\sqrt{\text{Hz}}$ .

We operated the instrument in the nominal on-orbit configuration; i.e., He filled in the He tank, cryocoolers operated at nominal power, and the VIS launch locks released. The detector performance was stable. We examined the detector response using a fixed  $f_{\text{STC}} = 15.0$  Hz while varying  $f_{\text{JTC}}$  on December 11. We first moved from  $f_{\text{JTC}} = 52.0$  Hz upward to 53.8 Hz, and then restarted from 52.0 Hz and moved downward to 50.4 Hz. At each step, we dwelled for 5 minutes and measured the detector noise spectra and the accelerometer spectra.

### 4 Results

Fig. 2 shows (a) the accelerometer spectra in the  $z$ -axis of the He tank and (b) the detector noise spectra for a representative detector pixel (pixel 0) in the 0–500 Hz range. In (a), the fundamental and harmonics of the fixed  $f_{\text{STC}}$  and varying  $f_{\text{JTC}}$  are observed for multiple orders across the frequency range. This is not surprising for mechanical coupling from the cryocoolers. However, the propagation of these into the detector noise in (b) exhibits several interesting features, which are also observed in other combinations of the accelerometer channels ( $x$ ,  $y$ , and  $z$  of the He tank) and detector channels (pixels 0–35).

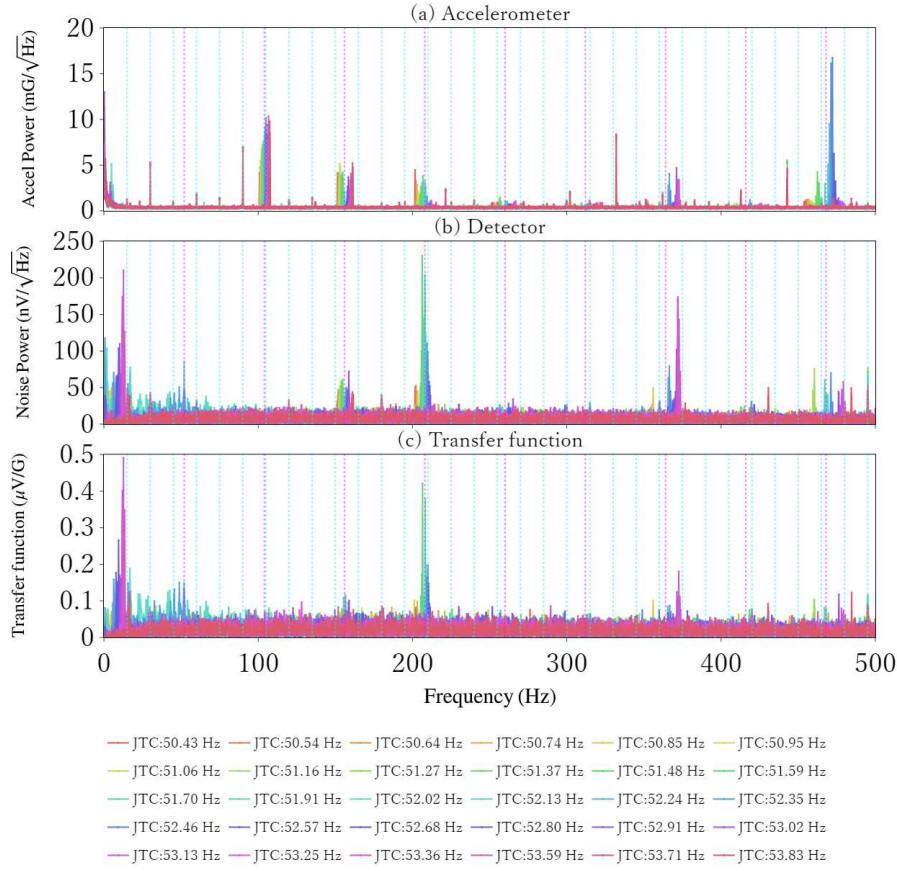


**Fig. 2** (a) Accelerometer spectra in the  $z$ -axis of the He tank. (b) Detector noise spectra for pixel 0. (c) Transfer function derived from (b)/(a) by matching the frequency resolution. Different colors indicate different  $f_{\text{JTC}}$  settings. The fundamental and harmonics of  $f_{\text{STC}} = 15.0$  Hz and  $f_{\text{JTC}} = 52.0$  Hz are shown with dotted cyan and magenta lines, respectively.

First, the frequency of the detector line noise changes as  $f_{\text{JTC}}$  changes. This is particularly evident for  $n_{\text{JTC}} = 3, 4, 7,$  and  $9$  for the  $n_{\text{JTC}}$ 'th harmonics. This indicates the JTC origin for these lines. Second, the amplitude of the interference lines is very different between different  $n_{\text{JTC}}$ 's:  $n_{\text{JTC}} = 2$  and  $3$  are the strongest in the accelerometer spectra, but  $n_{\text{JTC}} = 4$  and  $7$  are the strongest in the detector noise spectra. Third, the detector noise at  $f_{\text{JTC}}$  and below is enhanced only when the JTC-drive frequency is close to  $52.0$  Hz as shown in blue in (b). Fourth, line noise is present in the low- $f$  range ( $\lesssim 20$  Hz) in the detector noise spectra (b). These effects all originate from the cryocoolers as their frequency and intensity change as  $f_{\text{JTC}}$ . However, the low- $f$  lines are absent in the accelerometer spectra (a).

Fig. 3 is another representation of the third and fourth features discussed above. The intensity of the detector noise (pixel 0) as a function of  $f_{\text{JTC}}$  is shown with a heat map. These data were acquired when  $f_{\text{STC}}$  was  $15$  Hz. The noise caused by the STC drive frequency appears as horizontal lines at  $15$  Hz (faint) and  $30.0$  Hz, while those due to the JTC as

vertical lines are most evident at  $f_{\text{JTC}} = 52.0\text{--}52.4$  Hz. In addition, we see many diagonal lines. From the slope, these are associated with  $n_{\text{JTC}} = 4$  and 7. Furthermore, from the absolute values of the changing frequencies, we found that they are the beat frequencies represented by  $f_{\text{beat}} = |n_{\text{JTC}}f_{\text{JTC}} - n_{\text{STC}}f_{\text{STC}}|$ , in which  $n_{\text{STC}} = 14$  (and 15 for a weak signal) for  $n_{\text{JTC}} = 4$  and  $n_{\text{STC}} = 24$  (and 23 with a weak signal) for  $n_{\text{JTC}} = 7$ . The beat only appears, in particular,  $f_{\text{JTC}}$  ranges. Beat lines for other  $n_{\text{JTC}}$ 's were not observed, which is interesting as there is always a matching  $n_{\text{STC}}$  that makes  $f_{\text{beat}} < 20$  Hz for all  $n_{\text{JTC}}$ 's.

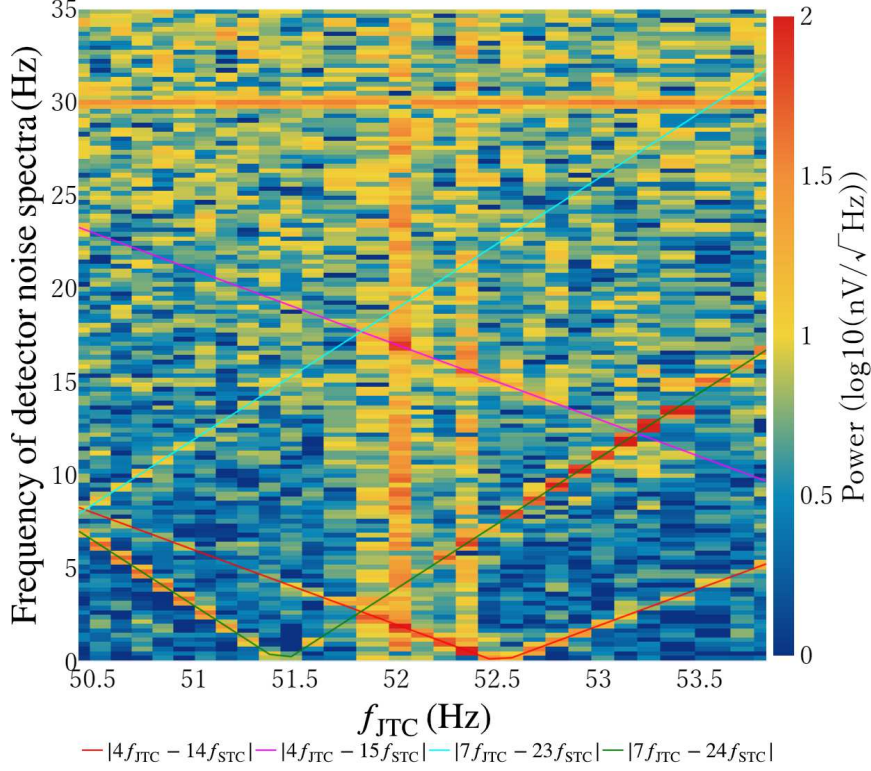


**Fig. 3** Detector noise spectra (pixel 0) shown in a heat map as a function of  $f_{\text{JTC}}$ . Beat lines calculated by  $f_{\text{beat}} = |n_{\text{JTC}}f_{\text{JTC}} - n_{\text{STC}}f_{\text{STC}}|$  are shown in different colors.

There should be some physical mechanisms to explain why the beat frequency lines appear in the detector noise spectra since linear combinations of  $n_{\text{JTC}}f_{\text{JTC}}$  and  $n_{\text{STC}}f_{\text{STC}}$  tones cannot redistribute power into the  $f_{\text{beat}}$  tone. Assuming that  $f_1 = n_{\text{JTC}}f_{\text{JTC}}$  and  $f_2 = n_{\text{STC}}f_{\text{STC}}$  tones ( $A_1$  and  $A_2$ , respectively) are linearly mixed with the same phase and amplitude of unity, the mixture ( $A_{12}$ ) is

$$\begin{aligned} A_{12} &= A_1 + A_2 = \cos(2\pi f_1 t) + \cos(2\pi f_2 t) = 2 \cos\left(2\pi \frac{f_1 - f_2}{2} t\right) \cos\left(2\pi \frac{f_1 + f_2}{2} t\right) \\ &= 2 \cos(2\pi f_{\text{mod}} t) \cos(2\pi f_{\text{carrier}} t). \end{aligned}$$

The mixed signal is the amplitude modulation of the single carrier frequency  $f_{\text{carrier}} = (f_1 + f_2)/2$  with the modulation frequency  $f_{\text{mod}} = (f_1 - f_2)/2 = f_{\text{beat}}/2$ . The Fourier transform of  $A_{12}$  has power only at the  $f_1$  and  $f_2$  tones and not at the  $f_{\text{beat}}$  tone. However, when a non-linear effect takes place on  $A_{12}$  to become  $A'_{12}$ , such as a one-sided clip ( $A'_{12} = \min(A_{12}, A_{12,\text{thres}})$ , where  $|A_{12,\text{thres}}| < 2$ ) or a cubic term ( $A'_{12} = \alpha^{(1)}A_{12} + \alpha^{(3)}A_{12}^3$ , where  $\alpha^{(1,3)}$  are coefficients), the power is redistributed into  $f_{\text{beat}}$  and its harmonic tones. It is not relevant for the redistribution whether a non-linear effect takes place in each of  $A_1$  or  $A_2$ . Only non-linear effect of  $A_{12}$  produces the redistribution.

We speculate as follows. When both  $f_1$  and  $f_2$  are close to resonance frequencies, their tones are amplified. This only occurs for particular  $n_{\text{JTC}}$ 's and  $n_{\text{STC}}$ 's in order to explain why the beat appears only for ( $n_{\text{JTC}}=4$ ,  $n_{\text{STC}}=14$  and weakly 15) and ( $n_{\text{JTC}}=7$ ,  $n_{\text{STC}}=24$  and weakly 23) and in particular  $f_{\text{JTC}}$  ranges. In fact, for these  $n_{\text{JTC}}$ 's and  $n_{\text{STC}}$ 's, some resonances are estimated from mechanical models: 209 Hz for the ADR salt pill and 372 Hz for the detector assembly. The beat from  $n_{\text{JTC}} = 4$  (Fig. 3) disappears at  $f_{\text{JTC}} < 51.6$  Hz presumably because  $4f_{\text{JTC}}$  is too far from 209 Hz. The beat from  $n_{\text{JTC}} = 7$  appears in two parts:  $f_{\text{JTC}} < 51.5$  and  $> 52.0$  Hz, suggesting that there are two beat frequencies at  $\sim 355$  and 372 Hz. A non-linear effect, though its exact physical mechanism is still unknown, must take place in the mixed signal of the two amplified monotonics, which then redistributes power into the  $f_{\text{beat}}$  tone. Another possible origin of the  $f_{\text{beat}}$  tone is the sensitivity of the detector on the amplitude of the modulation  $|\cos(2\pi f_{\text{mod}} t)|$ .

The observed phenomena are specific to the *Resolve* instrument, but the resonance at one of the cryocooler harmonics and a non-linear response can occur in any instrument. The resultant power redistribution into the low- $f$  range may cause a serious challenge for the performance of low temperature detectors regardless of whether they are employed for calorimetric or bolometric use. We have described one such case observed during a ground test of *Resolve*. Some lessons for future missions can be learned from this experiment: (1) a single tone sweep test may be insufficient to understand micro-vibration phenomena, (2) tests of highly integrated systems are required to characterize the effects, and (3) flexibility of drive frequencies may allow to mitigate the interference at late stages of the project.

## 5 Summary

Here, we have given a brief description of the microphonic noise in the detector signal caused by the cryocoolers during a ground test of the *Resolve* instrument. Not only the fundamental and harmonics of the cryocoolers driven at 15.0 and 52.0 Hz were observed, but we also observed the low frequency ( $< 20$  Hz) line noise corresponding to the beat frequency of some combinations of the harmonics of the two driving frequencies. We have discussed that some of these effects correspond to the known resonance frequencies of the instrument and that a non-linear behavior must be occurring to account for power redistributed into the beat frequency tone.

**Acknowledgements** This study was made possible by the collaborative efforts of all members of the *Resolve* team, including Sumitomo Heavy Industries, which we greatly appreciate.

## References

1. Mitsuda, K., et al. *Proceedings of SPIE* **9144**, (2014), DOI:10.1117/12.2057199



2. Kelley, R. L., et al. *Proceedings of SPIE* **9905**, (2016), DOI:10.1117/12.2232509
3. Takahashi, T., et al. *Proceedings of SPIE* **9905**, (2016), DOI:10.1117/12.2232379
4. Takei, Y., et al. *Journal of Astronomical Telescopes, Instruments, and Systems* **4**, 1, 011216 (2018), DOI:10.1117/1.jatis.4.1.011216
5. Porter, F. S., et al. *Journal of Astronomical Telescopes, Instruments, and Systems* **4**, 1, 011218 (2018), DOI:10.1117/1.jatis.4.1.011218
6. Leutenegger, M. A., et al. *Journal of Astronomical Telescopes, Instruments, and Systems* **4**, 2, 021407 (2018), DOI:10.1117/1.jatis.4.2.021407
7. Tashiro, M. S., et al. *Proceedings of SPIE* **11444** (2020), DOI:10.1117/12.2565812
8. Ezoe, Y., et al. *Cryogenics* **108**, 103016 (2020), DOI:10.1016/j.cryogenics.2019.103016
9. Ishisaki, Y., et al. *Proceedings of SPIE* **12181**, in press
10. Imamura, R., et al. *Proceedings of SPIE* **12191**, in press
11. Hasebe, T., et al. *Proceedings of SPIE* **12181**, in press
12. Kilbourne, C. A., et al. *Journal of Astronomical Telescopes, Instruments, and Systems* **4**, 1, 011214 (2018), DOI:10.1117/1.jatis.4.1.011214
13. Shirron, P. J., et al. *Journal of Astronomical Telescopes, Instruments, and Systems* **4**, 2, 021403 (2018), DOI:10.1117/1.jatis.4.2.021403
14. Chiao, M. P., et al. *Journal of Astronomical Telescopes, Instruments, and Systems* **4**, 1, 021404 (2018), DOI:10.1117/1.JATIS.4.2.021404
15. Yoshida, S., et al. *Journal of Cryogenics and Superconductivity Society of Japan* **53**, 6, 349 (2018), DOI:10.2221/jcsj.53.349
16. Fujimoto, R., et al. *Journal of Astronomical Telescopes, Instruments, and Systems* **4**, 1, 011208 (2018), DOI:10.1117/1.jatis.4.1.011208
17. Sneiderman, G. A., et al. *Journal of Astronomical Telescopes, Instruments, and Systems* **4**, 2, 021408 (2018), DOI:10.1117/1.jatis.4.2.021408
18. Sato, Y., et al. *Cryogenics* **52**, 4–6, 158, (2010), DOI:10.1016/j.cryogenics.2012.01.026

This figure "f01e.jpg" is available in "jpg" format from:

<http://arxiv.org/ps/2303.01004v1>



This figure "f02c.jpg" is available in "jpg" format from:

<http://arxiv.org/ps/2303.01004v1>

This figure "f03b.jpg" is available in "jpg" format from:

<http://arxiv.org/ps/2303.01004v1>